JOURNAL OF THE KOREAN ASTRONOMICAL SOCIETY
38: 191 ~ 195, 2005

THE MASS PROFILE OF ABELL 1689 FROM A LENSING ANALYSIS OF DEEP WIDE FIELD SUBARU IMAGES

KEIICHI UMETSU[1], TOM BROADHURST[2], MASAHIRO TAKADA[3], AND XU KONG[4]
[1]Institute of Astronomy and Astrophysics, Academia Sinica, P. O. Box 23-141, Taipei 106, Taiwan, R.O.C.
E-mail: keiichi@asiaa.sinica.edu.tw
[3]School of Physics and Astronomy, Tel Aviv University, Israel
E-mail: tjb@wise1.tau.ac.il
[2]Astronomical Institute, Tohoku University, Sendai 980-8578, Japan
E-mail: takada@astr.tohoku.ac.jp
[4]National Astronomical Observatory of Japan, Mitaka 181-8588, Japan
E-mail: xkong@optik.mtk.nao.ac.jp
(Received February 1, 2005; Accepted March 15, 2005)

ABSTRACT

We used Subaru observations of A1689 ($z = 0.183$) to derive an accurate, model-independent mass profile for the entire cluster, $r \lesssim 2\mathrm{Mpc}/h$, by combining magnification bias and distortion measurements. The projected mass profile steepens quickly with increasing radius, falling away to zero at $r \sim 1.0\mathrm{Mpc}/h$, well short of the anticipated virial radius. Our profile accurately matches onto the inner profile, $r \lesssim 200\mathrm{kpc}/h$, derived from deep HST/ACS images. The combined ACS and Subaru information is well fitted by an NFW profile with virial mass, $(1.93 \pm 0.20) \times 10^{15} M_{\odot}$, and surprisingly high concentration, $c_{\mathrm{vir}} = 13.7^{+1.4}_{-1.1}$, significantly larger than theoretically expected ($c_{\mathrm{vir}} \simeq 4$), corresponding to a relatively steep overall profile. These results are based on a reliable sample of background galaxies selected to be redder than the cluster E/S0 sequence. By including the faint blue galaxy population a much smaller distortion signal is found, demonstrating that blue cluster members significantly dilute the true signal for $r \lesssim 400\mathrm{kpc}/h$. This contamination is likely to affect most weak lensing results to date.

Key words : cosmology: observations – gravitational lensing – galaxy clusters: individual (Abell 1689)

I. INTRODUCTION

Numerical simulations based on the cold dark matter (CDM) scenario are reliable enough to make statistical predictions for the mass profiles of clusters. The gradient of an 'NFW' profile is predicted to monotonically steepen with increasing radius (Navarro, Frenk & White 1997), with logarithmic slopes shallower than an isothermal profile interior to the characteristic radius $r < r_s$, but steeper at larger radius, approaching to r^{-3} at $r \to r_{\mathrm{vir}}$. This curvature is particularly pronounced for massive clusters, where the halo is expected to have a relatively low concentration, providing a clear prediction. Weak lensing work has yet to make a definitive statement regarding the validity of the NFW profile, with the analysis claiming only broad consistency with both the singular isothermal case and the NFW model (Clowe & Schneider 2001; Bardeau et al. 2004).

Recently, the central region of A1689 ($z = 0.183$) has been imaged in detail with the Advanced Camera for Surveys (ACS), revealing 106 multiply lensed images of 30 background galaxies (Broadhurst et al. 2004, B04). Many radially directed images define a radial critical curve, inside which small counter-images are identified, so the mass profile can be traced in detail to the center of mass. An NFW profile fits well over the restricted ACS field, $r \lesssim 200\mathrm{kpc}/h$, but with a somewhat larger concentration, $c_{\mathrm{vir}} = 8.2^{+2.1}_{-1.8}$, than expected for massive clusters, $c_{\mathrm{vir}} \sim 4$ (e.g., Bullock et al. 2001). To examine the shape of the full profile, we turn to the wide-field prime focus camera, Suprime-Cam, of the 8.2m Subaru telescope. Suprime-Cam provides an unparalleled combination of area ($34' \times 27'$) and depth (Miyazaki et al. 2002). We measure the lensing distortion and magnification of background red galaxies and combine them to derive a model-independent mass profile out to $r \sim 2\mathrm{Mpc}$, allowing a definitive comparison with model profiles. Throughout this paper, the concordance ΛCDM cosmology is adopted ($\Omega_{\mathrm{m0}} = 0.3$, $\Omega_{\lambda 0} = 0.7$, $h = 0.7$). Note that one arcminute corresponds to the physical scale $129\mathrm{kpc}/h$ for this cluster. The main results of this paper were reported in Broadhurst, Takada, Umetsu et al. (2005: B05b).

Proceedings of *the 6th East Asian Meeting of Astronomy*, held at Seoul National University, Korea, from October 18-22, 2004.

II. DATA REDUCTION AND SAMPLE SELECTION

Suprime-Cam imaging data of A1689 in V (1,920s) and SDSS i' (2,640s) were retrieved from the Subaru archive, SMOKA. Reduction software developed by Yagi et al (2002) was used for flat-fielding, instrumental distortion correction, differential refraction, PSF matching, sky subtraction and stacking. The resulting FWHM is $0''.82$ in V and $0''.88$ in i' with $0''.202$ pix^{-1}, covering a field of $30' \times 25'$. Photometry is based on a combined $V + i'$ image using SExtractor (Bertin & Arnaut 1996). The limiting magnitudes are $V = 26.5$ and $i' = 25.9$ for a 3σ detection within a $2''$aperture (we use the AB magnitude system). For the number counts to measure magnification, we define a sample of 8,907 galaxies (12.0 arcmin^{-2}) with $V - i' > 1.0$. For distortion measurement, we define a sample of 5,729 galaxies (7.59 arcmin^{-2}) with colors 0.22 mag redder than the color-magnitude sequence of cluster E/S0 galaxies, $(V - i') + 0.0209i' - 1.255 > 0.22$. The smaller sample is due to the fact that distortion analysis requires galaxies used are well resolved to make reliable shape measurement. We adopt a limit of $i' < 25.5$ to avoid incompleteness effect. Our red galaxies are very reasonably expected to lie behind the cluster, made redder by larger k-corrections. The counts of all galaxies including the dominant faint blue population is much larger, $\sim$ 40 arcmin^{-2}. However, as we show below, the distortion signal of the full sample is significantly diluted within $r \lesssim 400$kpc$/h$, compared to the red sample, indicating that blue cluster members contaminate the sample. The mean redshift of the red galaxies is estimated to be $z_s \simeq 1 \pm 0.1$, based on deep photo-z estimation for deep field data (Benitez et al. 2002). In the following we will assume $\langle z_s \rangle = 1$ for the mean redshift, but note that the low redshift of A1689 means that for lensing work, a precise knowledge of this redshift is not critical.

III. LENSING DISTORTIONS

We use the IMCAT package developed by N. Kaiser for our distortion analysis, following the well tested formalism outlined in Kaiser, Squires & Broadhurst (1995), with modifications described by Erben et al. (2001). Figure 1. shows the radial profiles of the tangential distortion, g_+, and the 45-degree rotated ($\times$) component, $g_\times$, for the different samples of galaxies, where the cluster center is well determined by the locations of brightest cluster galaxies and/or giant arcs. Note that lensing induces only the tangential shear in the weak lensing regime. It is clear that the observed signal is significant to the limit of our data, $\sim 20'$ or 2Mpc$/h$, and that the $\times$-component of the red galaxy sample is consistent with a null signal at all radii, indicating the reliability of our distortion analysis. One can see that the NFW prediction for source redshift $z_s = 1$ ($c_{\rm vir} = 8.2$ and $M_{\rm vir} = 2.6 \times 10^{15} h M_\odot$), which fits best

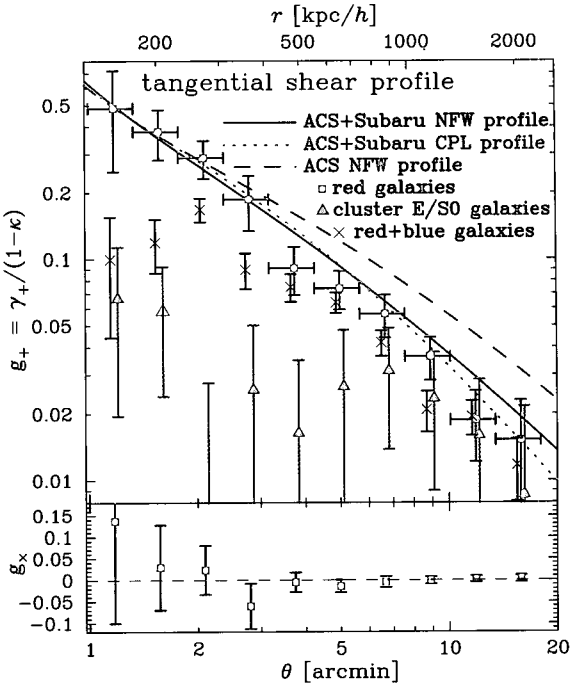

Fig. 1.— Radial profiles of the tangential shear (upper panel) and the 45° rotated ($\times$) component (lower panel). The square symbols correspond to the red background sample. The cross symbols correspond to the full sample of faint red+blue galaxies, excluding objects falling on the narrow cluster E/S0 sequence. The triangle symbols denote galaxies with photometry coincident with the color-magnitude sequence of cluster E/S0 galaxies. The solid and dotted curves show an NFW profile with a large concentration, $c_{\rm vir} \approx 14$, and a power-law profile with slope $n = 3.16$ and core $\theta_c = 1.65$ arcmin (see §V), respectively, both matching well the overall profile of the red galaxy sample. The best-fitting model (dashed curve) based on the inner ACS measurements (B04), with $c_{\rm vir} \simeq 8$, clearly overestimates the outer profile.

the ACS strong lensing data restricted to the central region $\lesssim 2'$ (B04), matches onto the Subaru distortions at $\lesssim 3'$ for the background red galaxies, but increasingly overestimates the distortions at larger radii $\gtrsim 3'$. A steeper NFW profile with $c_{\rm vir} \sim 14$ (solid curve) better reproduces the distortion profile at all radii, as does a cored power-law profile (dotted curve), (see §V for the details).

A careful background selection is critical. If we select all galaxies irrespective of color with magnitude limit $i' < 25.5$, and exclude only the cluster sequence galaxies, then we find that the distortion signal falls below the red background sample by a factor of 2-5 at $r \lesssim 400$kpc$/h$. While the slight dilution within a factor of 2 is still apparent at large radii $\gtrsim 5'$, blue cluster members must be significantly contaminating the full sample at the small radii, reducing the distortion signal.

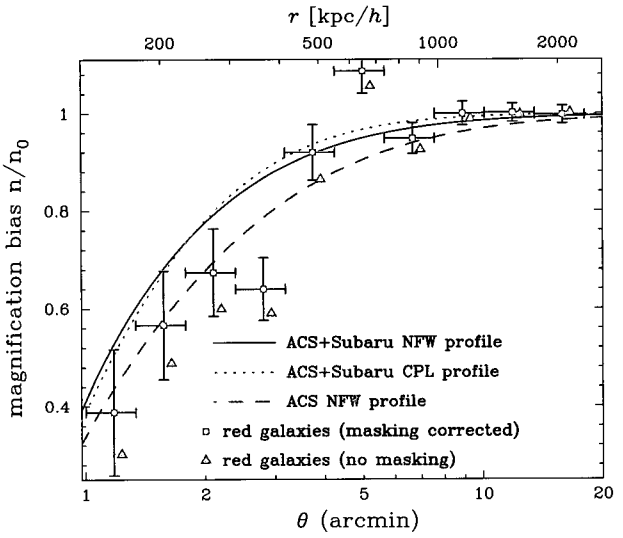

Fig. 2.— Number-count profile of the red background galaxies (square symbols). The triangle symbols show the counts without the mask correction due to cluster members. The model curves are shown for comparison as in Figure 1.

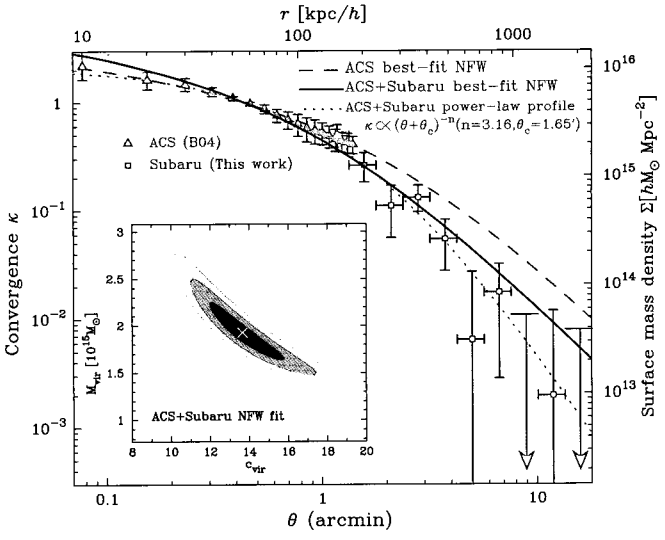

Fig. 3.— Reconstructed mass profile. The triangle and square symbols with error bars show the results from the ACS strong lensing analysis (B04) and the Subaru weak lensing analysis (this work), respectively. The dashed and solid curves show the best-fitting NFW profiles for the ACS data alone and for the combined ACS+Subaru profile, respectively.

IV. MAGNIFICATION BIAS

Lensing magnification, $\mu(\vec{\theta})$, influences the observed surface density of background galaxies, expanding the area of sky, and enhancing the flux of galaxies (BTP). The number counts for a given magnitude cutoff $m_{\rm cut}$, approximated as a power law with slope $s \equiv d\log N_0/dm$, are modified as $N(< m_{\rm cut}) = N_0(< m_{\rm cut})\mu^{2.5s-1}$, where N_0 is the unlensed counts. Thanks to the large Subaru FOV, the normalization and slope of N_0 for our red galaxy sample are reliably estimated as $n_0 = 12.6\pm0.23$ arcmin^{-2} and $s = 0.22\pm0.03$ from the outer region $\geq 10'$. The slope is less than the lensing invariant slope, $s = 0.4$, so a net deficit of background galaxies is expected. The number density in each radial annulus is then calculated by excluding this area and simply renormalising. Note that, if we adopt the masking factor of 2 or 4 instead of 3, the results shown below are little changed. Figure 2 shows that the red galaxy counts are clearly depleted, with a clear trend towards higher magnification in the center. The masking area is negligible at large radius and rises to $\sim 20\%$ of the sky close to the center, $r \lesssim 3'$. Comparison with models shows that the data are broadly in agreement with the profiles as described in §V. We have ignored the intrinsic clustering of background galaxies, which seems a good approximation, though some variance is apparent in 2D maps (Umetsu et al. 2004 in preparation) and may explain a discrepant point at $\sim 5'$ in the radial profile.

V. MODEL-INDEPENDENT MASS PROFI -LE

The relation between distortion and convergence is non-local, and masses derived from distortion data alone suffers from a mass sheet degeneracy. However, by combining the distortion and magnification measurements the convergence can be obtained unambiguously. Here we derive a model-independent, discrete convergence profile in 10 logarithmically spaced bins for $1' \leq \theta \leq 18'$: $\kappa_i \equiv \kappa(\theta_i)$ for $i = 1, 2, \ldots, 10$, representing 10 free parameters which are constrained with 20 data points in Figures 1 and 2. To perform the mass reconstruction, we need to express the lensing observables in terms of the binned convergence profile. The tangential shear amplitude in the i-th radial bin can be expressed as $\gamma_{+i} = \bar{\kappa}_i - \kappa_i$ (Fahlman et al. 1994), where $\bar{\kappa}_i$ is the average convergence interior to radius θ_i and expressed as $\bar{\kappa}_i \equiv \bar{\kappa}(\theta_i) = 2/\theta_i^2 \sum_{j=1}^{i} \theta_j^2 \kappa_j h$ with the bin width $h \equiv \Delta \ln\theta$. Once the shear profile is given, it is straightforward to compute the binned tangential distortion and magnification via the relations $g_{+i} = \gamma_{+i}/(1-\kappa_i)$ (at radii of our interest) and $\mu_i = |(1-\kappa_i)^2 - \gamma_{+i}^2|^{-1}$. However, for the discrete model, to properly compute the shear in the first bin, we need to specify the mass interior to radius $1'$, which is readily obtained from the well constrained ACS derived profile. We have checked that, if we instead adopt the model independent mass interior to the Einstein radius ($\approx 45''$), the results are very similar.

The best-fitting model κ_i is then derived by properly weighting signal-to-noise (S/N) ratios of the distortion and magnification data (e.g., see Schneider, King & Erben 2000). The square symbols in Figure 3 show the best-fitting mass profile obtained from the Subaru data, where the minimized χ^2 value is $\chi^2_{\rm min}/{\rm dof.} = 27.9/10$ for 10 degrees of freedom. The bad $\chi^2_{\rm min}$ is mainly

due to the two data points at $\sim 3'$ and $5'$ in Figure 2, which apparently deviate from a continuous curve and are probably affected by the intrinsic clustering of background galaxies. Excluding the two data points leads to an acceptable fit $\chi^2_{\rm min}/{\rm dof.} = 12.4/8$, meaning the best-fit mass profile well reproduces the distortion and magnification data simultaneously. The outer profile at $\theta \gtrsim 9'$ is consistent with a null signal to within 1σ (the points at $\sim 9'$ and $16'$ are 1σ upper limits), implying a more rapid decay in mass profile than expected from the standard NFW profile, falling well short of the anticipated virial radius. We have also checked that this result is not sensitive to varying the count-slope and the unlensed background galaxy density within the 1σ measurement errors. Force fitting an NFW profile to the Subaru mass profile yields $M_{\rm vir} = 1.69^{+0.30}_{-0.28} \times 10^{15} M_\odot$ ($r_{\rm vir} = 1.95 \pm 0.11{\rm Mpc}/h$) for the virial mass (radius), where $\chi^2_{\rm min}/{\rm dof.} = 5.36/8$. Note that the NFW profile is specified by the two parameters, $M_{\rm vir}$ and halo concentration $c_{\rm vir}$ (Bartelmann 1996), and we have adopted the flat prior $c_{\rm vir} \leq 30$ because the NFW profiles with $c_{\rm vir} \gtrsim 20$ can not be distinguished by the Subaru data alone due to lack of information on the inner density profile. The error quotes 68% confidence intervals ($\Delta\chi^2 \equiv \chi^2 - \chi^2_{\rm min} \leq 1$). Next, we consider the combined Subaru and ACS profile, where the ACS profile with error bars is taken from Figure 22 in B04 and the amplitude is scaled to $z_s = 1$ from the $z_s = 3$ result. By combining the strong and weak lensing analyses, we can trace the mass distribution over a large range in amplitude $\kappa \sim [10^{-3}, 1]$ and in radius $r = [10^{-2}, 2]{\rm Mpc}/h$. In this case, we have 22 independent data points in total excluding the ACS data points at radii overlapping with the Subaru data. The best-fitting NFW profile is given by $c_{\rm vir} = 13.7^{+1.4}_{-1.1}$ and $M_{\rm vir} = (1.93 \pm 0.20) \times 10^{15} M_\odot$ ($r_{\rm vir} = 2.04 \pm 0.07{\rm Mpc}/h$), and has an acceptable fit $\chi^2_{\rm min}/{\rm dof.} = 13.3/20$. The inset plot shows how the constraints are degenerate in the ($c_{\rm vir}$, $M_{\rm vir}$) plane. Hence, this result gives the lensing based confirmation of the NFW profile over the radii we have considered, however, the mass distribution appears to be much more concentrated toward the center than the CDM simulations predict for a halo of the above mass, $c_{\rm vir} = 4.0$ (Bullock et al. 2001). A generalized NFW profile given by $\rho \propto r^{-1.5}(1 + r/r_s)^{-1.5}$ (e.g., Moore et al. 1998) is disfavored ($\chi^2_{\rm min}/{\rm dof.} = 28.3/20$; see Umetsu et al. 2004 for more details), being too steep in the center. A cored power-law profile, $\kappa \propto (\theta + \theta_c)^{-n}$, gives a better fit: $\chi^2_{\rm min} = 4.49/19$ with a steep slope, $n = 3.16^{+0.81}_{-0.72}$, and a core of $\theta_c = 1.65^{+0.77}_{-0.61}$ arcmin ($r_c = 214^{+99}_{-78}$ kpc/h). A softened isothermal profile is strongly rejected (10σ level!).

VI. DISCUSSION AND CONCLUSION

We have obtained a secure, model-independent mass profile of A1689 over $1' < \theta \lesssim 20'$ ($100{\rm kpc}/h \lesssim r \lesssim 2{\rm Mpc}/h$) by combining the distortion and magnification-bias measurements from high-quality Subaru imaging. We have seen that to reliably measure distortions it is critically important to securely select background galaxies in order to avoid dilution of the distortion signal by blue cluster members and foregrounds (see Figure 1). Thus we have resolved the discrepancy between the small Einstein radius ($\sim 20''$) inferred from the previous work based on largely monochromatic measurements and the observed radius ($\sim 45''$). The mass profile of A1689 obtained from the Subaru and ACS data covers 2 orders of magnitude in radius, $[10^{-2}, 2]{\rm Mpc}/h$, and shows a continuously steepening profile with increasing radius, very similar to an NFW profile but with a much higher concentration than expected. The best-fitting NFW profile has $c_{\rm vir} \simeq 14$, significantly larger than expected $c_{\rm vir} \simeq 4$, corresponding to the profile expected for a much lower mass halo of $\sim 10^{11-12} M_\odot$ (Bullock et al. 2001), 3-4 orders of magnitude less than the mass of A1689. Subaru imaging in more passbands will provide many reliable photometric redshifts for refining the background selection, helping to improve the distortion signal and allowing the lens magnification to be separated from the background clustering. In addition, the redshift dependence of the distortion and magnification signals may be extracted to constrain cosmological parameters.

ACKNOWLEDGEMENTS

This work is based on the collaboration with N. Arimoto, M. Chiba, and T. Futamase. Part of this work is based on data collected at the Subaru Telescope, which is operated by the National Astronomical Society of Japan.

REFERENCES

Bardeau, S., Kneib, J.-P., Czoske, O., Soucail, G., Smail, I., Ebeling, H., 2004, astro-ph/0407255

Bartelmann, M., 1996, A&A, 313, 697

Bertin, E., & Arnouts, S., 1998, A&AS, 117, 393

Broadhurst, T. J., et al., 2005, ApJ, 621, 53 (B05a)

Broadhurst, T. J., et al., 2005, ApJ, 619, 143L (B05b)

Bullock, J. S., et al., 2001,

MNRAS, 321, 559

Clowe, D., & Schneider, P., 2001, A&A, 379, 384

Erben, T., Van Waerbeke, L., Bertin, E., Mellier, Y., & Schneider, P., 2001, A&A, 366, 717

Fahlman, G., Kaiser, N., Squires, G., & Woods, D., 1994, ApJ, 437, 56

Kaiser, N., Squires, G., & Broadhurst, T., 1995, ApJ, 449, 460

Miyazaki, S., et al., 2002, PASJ, 54, 833

Moore, B., Governato, F., Quinn, T., Stadel, J., & Lake G., 1998, ApJ, 499, L5

Navarro, J. F., Frenk, C. S., & White, S. D. M., 1997, ApJ, 490, 493

Schneider, P., King, L., & Erben, T., 2000, A&A, 353, 41

Yagi, M., Kashikawa, N., Sekiguchi, M., et al., 2002, AJ, 123, 66